High aspect ratio Ge-on-Si waveguide platform for miniaturized mid-infrared applications

Andrew Whye Keong Fong[a], Rachel Chen Fang Ang[a], Leh Woon Lim[a], Lennon Yao Ting Lee[a], Qingxin Zhang[a], Doris Keh Ting Ng[a], Xianshu Luo[a], Landobasa Y.M. Tobing*[a]

[a]Institute of Microelectronics (IME), Agency for Science, Technology and Research (A*STAR), 2 Fusionopolis Way, Innovis #08-02, Singapore 138634, Republic of Singapore

ABSTRACT

On-chip spectrometer operating in the mid-infrared (MIR) regime (λ = 2 – 14 µm) enables the miniaturization of a chemical sensing platform that identifies compounds based on their unique molecular fingerprints. Germanium-on-Silicon (Ge-on-Si) material system is a suitable candidate for its transparency in the MIR spectrum and compatibility with silicon processing. As chemical sensing is conducted by having the mode evanescent field interacting with the analyte, the design of Ge-on-Si waveguide for a compact footprint (small bending radius) and large evanescent field coverage is necessary. However, the bending radius of the Ge-on-Si waveguide is limited to hundreds of micrometers due to the low refractive index contrast between germanium and silicon. In this work, we demonstrate a 3 µm thick Ge-on-Si waveguide, with ~89° sidewall angles and a high gap aspect ratio of 10 (resolvable gaps of 300 nm). Different types of Ge-on-Si devices are fabricated including in-plane distributed Bragg grating (DBR) structures, cascaded Fabry-Perot resonators, and polarization splitters. We show that over-etching the Si lower cladding is able to reduce bending loss by ~10x, allowing us to decrease the bending radius to ~50 µm. Designs of 32 waveguide geometries for single mode propagation from 5.5 µm to 11 µm are presented, each of which is integrated with grating couplers operating at specific peak wavelengths. Our measurements show high consistency between the simulated and measured peak wavelengths of the grating couplers, with an inter-chip standard deviation of $\sigma_\lambda/\lambda_{peak}$ <1%.

Keywords: mid-infrared photonics, Germanium waveguide, propagation loss, sensing, Germanium-on-Silicon

1. INTRODUCTION

Non-dispersive infrared sensing (NDIR) is a chemical detection technique using wavelength-dependent fingerprint absorptions of different chemicals.[1,2] Compact and efficient NDIR sensing is highly relevant for distributed portable sensor networks, which find its potential applications in detecting toxic and flammable gases, such as methane (CH_4), ammonia (NH_3), and greenhouse gases[3-5] such as carbon dioxide (CO_2) and sulfur hexafluoride (SF_6). Employing optical waveguide as the photonic sensing medium enables the miniaturization of the NDIR sensing, where the interaction between the chemical analyte and the evanescent field of the guided mode gives rise to wavelength-specific absorptions unique to the chemicals. Germanium-on-Silicon (Ge-on-Si) material system is an excellent candidate for this application as Germanium (Ge) has a broad transparency from 2 µm to 15 µm,[6-11] while Silicon (Si) has a transparency range from 1.1 µm to 8 µm. Given the refractive index contrast (Δn) of Ge from Si of $\Delta n \sim 0.5$ it is possible to construct a mid-infrared (MIR) waveguide with Ge as the core and Si as the cladding, provided that the waveguide height is sufficiently tall to ensure the mode vertical confinement. However, such a large waveguide height (in contrast to the typical submicron thickness of a silicon-on-insulator waveguide) due to the smaller index contrast is also known to cause stronger lateral mode confinement, leading to a limited interaction of the mode fields with the chemical analyte. Meanwhile, decreasing the mode confinement could increase the interaction between the mode field and the analyte, but at the expense of increased propagation loss caused by either the inherent MIR absorption in the Si cladding or increased scattering loss on the waveguide sidewalls. This work aims to study Ge waveguide designs that address the sensing efficiency and propagation loss. Importantly, we study the role of the Si over-etch in reducing the bending loss and miniaturization of the sensing footprint. The fabrication of these designs is carried out by CMOS-compatible processes, with a waveguide height of 4 µm and a high aspect ratio gap spacing of 0.3 µm. Finally, the device characterizations are demonstrated, with excellent agreement with the numerical simulations.

* Landobasa_Tobing@ime.a-star.edu.sg; a-star.edu.sg/ime

2. GE-ON-SI WAVEGUIDE DESIGN AND FABRICATION

To minimize optical loss originating from threading dislocation defects, we designed our waveguide to be 3 μm thick such that the optical mode moves further away from the Si-Ge interfaces. The choice of this thickness also leads to increased loading effect of Ge towards the Si substrate, leading to increased transverse mode confinement. The fabrication of the Ge-on-Si waveguides was carried out by a standard silicon process comprising reduced pressure chemical vapor deposition (RPCVD) for Ge epitaxy, and multiple patterning for grating coupler and waveguide. The Ge-on-Si waveguide design is schematically shown in Fig. 1(a), showing input/output grating couplers with waveguide height of 3 μm and Si overetch depth of 1 μm. The role of Si over-etch is also explored in this work, which was found to provide additional transverse confinement that leads to reduced bending loss. The exemplary scanning electron microscopy (SEM) micrographs of the fabricated devices, accompanied by 1 μm Si overetch, are presented in Fig. 1(b), showing highly-vertical waveguides (with ~89° sidewall angle) and gap spacing as small as 300 nm (aspect ratio of ~10).

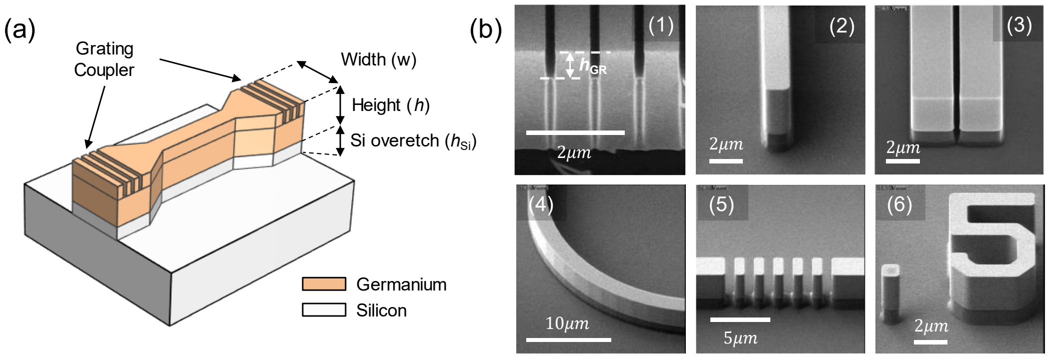

Fig. 1. (a) Schematic diagram showing Ge-on-Si waveguides integrated with input/output grating couplers. (b) Oblique angle SEM images of fabricated Ge-on-Si structures (in clockwise direction): (1) partially etched grating coupler with etch depth of h_{GR} = 1 μm, (2) waveguide (h = 3 μm and h_{Si} = 1 μm), (3) waveguides with gap spacing of g = 300 nm, (4) sidewall of bent waveguide, (5) fully etched in-line grating, (6) near-vertical etch profiles of h = 3 μm and h_{Si} = 1 μm.

The next aspect of the design is in determining the waveguide width that gives optimized evanescent field coverage for chemical sensing. The simulated mode index of Ge-on-Si waveguide at $\lambda = 6.5\ \mu m$ is shown in Fig. 2(a), showing TM_0 as the fundamental mode, followed by TE_0 as the higher order mode when the width is larger than 1.6 μm. The evanescent coverage is then estimated by calculating spatial field overlap in the air cladding for the TM_0 mode (gray curve), which shows a downward trend at increasing widths, which is expected from increased transverse mode confinement. However, while evanescent overlap can be increased by decreasing the waveguide width, it should be noted that this also leads to increased propagation loss (dashed curve). Such an increase in loss is caused by the proximity to the cutoff width for the fundamental mode and the increased overlap of the mode with Si lower cladding. In reality, the presence of sidewall roughness (resulting from the dry etching process) increases the loss at decreasing width more significantly as the enlarged mode field interacts with sidewall roughness and gives rise to sidewall scattering loss. Thus, there exists a trade-off between evanescent coverage and propagation loss which is estimated by $FoM = Overlap/Loss$, and plotted in Fig. 2(b) for different wavelengths. The peaks in the figure-of-merit (FoM) correspond to a specific waveguide width for optimized sensing in the presence of waveguide loss (as indicated by the dashed curve). We also note that the FoM peaks decrease as the wavelength is increased, suggesting the role of the MIR absorption in the Si in the increase of the propagation loss.

The role of Si overetch is investigated in Fig. 2(c), which presents simulated bending loss for Ge-on-Si waveguides with h_{Si} = 0 μm and h_{Si} = 1 μm. We observe that adding 1 μm Si overetch leads to an order of magnitude reduction in the bending loss, and a decrease of minimum bending radius from ~100 μm (for $h_{Si} = 0\ \mu m$) to ~50 μm (for $h_{Si} = 1\ \mu m$). The mode index of the TM_0 mode is not affected by Si overetch (and thus the evanescent overlap). However, the bending mode is affected by the Si overetch, as illustrated by the mode fields in Fig. 2(c). The bending mode for the Ge-on-Si waveguide without Si overetch appears to skew diagonally downward, which suggests the direction of the leakage loss (due to the bending). However, such a diagonally radiating leakage loss is blocked when Si overetch is introduced. This can be seen from a more symmetric bending mode profile for Ge-on-Si waveguide with $h_{Si} = 1\ \mu m$. In addition, the more symmetric bending mode translates to smaller minimum bending radius, as clearly seen in Fig. 2(c). Based on the optimum width for the figure of merit in Fig. 2(b), we design waveguide widths for 32 wavelength channels spanning from 5.5 μm to 11 μm, as shown in Fig. 2(d). The role of Si absorption in the waveguide loss is also simulated, showing a dramatic loss increase around 9 μm. Finally, grating couplers for these 32 wavelength channels are correspondingly designed for each waveguide.

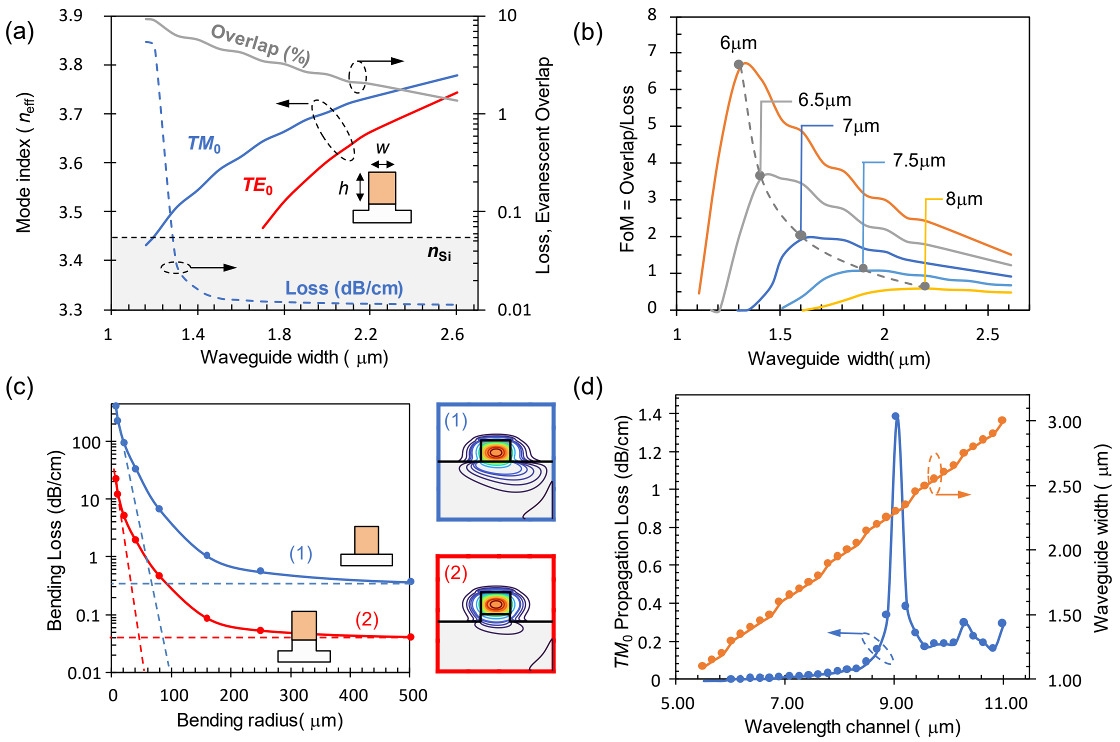

Fig. 2. (a) Simulated mode index and propagation loss (without consideration of sidewall roughness) of Ge-on-Si waveguides as a function of waveguide width for λ = 6.5μm. The refractive index of Si (n_{Si}) bottom cladding is denoted by the dashed line. The calculated spatial overlap of the evanescent field with the upper cladding (= air) is denoted by the gray curve (in percentage units). (b) The FoM of Ge-on-Si waveguide for sensing application, defined as the ratio between the evanescent field coverage with the analyte and the propagation loss. The FoM peaks for different wavelengths denote the optimum waveguide widths for sensing. (c) The bending loss for waveguides with h_{Si} = 0 μm, and h_{Si} = 1 μm, with their corresponding bend modes (at 40 μm bend radius). (d) The waveguide width for different wavelength channels for optimized sensing applications, with their simulated propagation loss (without sidewall roughness).

3. DEVICE CHARACTERIZATION

Ge-on-Si waveguides for 32 wavelength channels, integrated with grating couplers, were all fabricated within a single reticle. Dark field images of the fabricated S-bent Ge-on-Si waveguides are presented in Fig. 3(a), with the different dark field colors illustrating the different grating coupler pitches. The devices were characterized using a standard optical setup described in Fig. 3(b), which comprises quantum cascade lasers modulated by choppers, guided through hollow-core fibers into grating couplers, and a Mercury Cadmium Telluride (MCT) photodetector for data acquisition with a lock-in amplifier. The grating coupler responses for the 8 wavelength channels within the range of 5 μm to 11 μm were characterized. The peak wavelengths for each grating coupler response are presented in Fig. 3(c), with the linear line denoting the designed/calculated peak wavelength from finite difference time domain (FDTD) simulations. A good agreement between the experimental and simulation results is clearly observed, with peak wavelength standard deviation of $\sigma_\lambda/\lambda_{peak} < 1\%$. Propagation losses for different channels were measured from the cutback structures with waveguide lengths varied from 2 mm to 6 mm, showing wavelength-dependent waveguide loss from -4.2 ± 0.2 dB/cm to -37 ± 3.25 dB/cm for $\lambda = 5.5\ \mu m$ to $10.7\ \mu m$ (for $h_{Si} = 1.3\ \mu m$). The effect of Si overetch is also investigated in this case, showing propagation loss ranging from 1.4 ± 0.2 dB/cm to 31.1 ± 3.2 dB/cm for $\lambda = 5.5\ \mu m$ to $10.7\ \mu m$ (for $h_{Si} = 0.6\ \mu m$). Such a reduction in propagation loss is attributed to less dry etch-induced surface roughness from shorter process time.

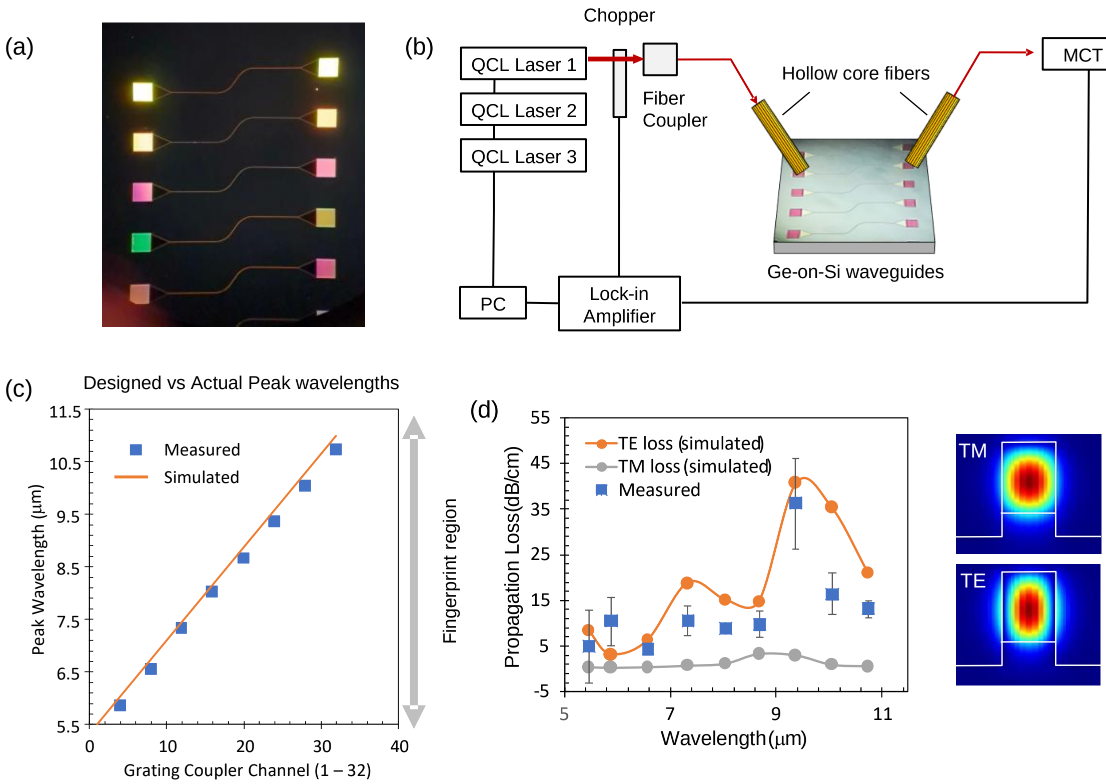

Fig. 3. (a) Dark field micrographs of the different S-bent waveguide structures integrated with grating couplers. The different grating pitches are illustrated in the different dark field colours. (b) Measurement setup of the Ge-on-Si samples. (c) Measured and simulated grating coupler peak wavelengths for the 32 waveguide channels spanning from 5.5μm to 11μm wavelength. (d) Measured propagation loss, in comparison with the simulated TE and TM losses in the presence of sidewall roughness.

The peak of the measured propagation loss is found around 9 μm, as expected from MIR absorption in Si and in a good agreement with the simulated propagation loss. Finally, as the incident polarization is unknown in the measurement, the role of polarization is also investigated to better understand the measured propagation loss. We simulated waveguide loss with sidewall roughness incorporated, with the root mean square roughness and correlation length chosen to be 5 nm and 10 nm, respectively. The simulated TM_0 and TE_0 propagation losses are presented in Fig. 3(d), which are significantly different from each other. This illustrates the different interaction between the guided modes and the sidewall roughness, as can be seen from the field profiles of TM_0 and TE_0 modes. For the TE_0 mode, the *E*-field is dominant in the horizontal direction, giving rise to large evanescent fields along the sidewall. In the presence of surface roughness, this results in large scattering loss, as evident in the much higher simulated TE_0 loss. Meanwhile, for TM_0 mode, the *E*-field is dominant in the vertical direction, and there is much less interaction between the evanescent field and the sidewall. This manifests in much smaller simulated TM_0 loss. Interestingly, our measured propagation loss is between the simulated TE_0 and TM_0 losses, suggesting that the incident polarization is a mixture of the two polarizations. We also note that, in addition to higher scattering loss for TE polarization, the higher order TE_0 mode is in the cutoff condition which translates to higher loss due to the mode leakage.

4. CONCLUSION

We have presented design and characterization of Germanium-on-Silicon waveguide devices aimed for chemical sensing applications. Despite the wide transparency of Ge as the waveguide core, the guided mode suffers from the MIR absorption in the Si lower cladding, particularly towards the longer wavelengths. This translates to a tradeoff between sensing efficiency (gauged by the evanescent field coverage) and propagation loss (due to the Si absorption and sidewall scattering loss). Based on this tradeoff, specific waveguide widths have been designed for optimized evanescent coverage for sensing, together with the grating couplers for the input/output interface. Our grating coupler characterization reveals good consistency with those from the simulations, with <1% standard deviation. Finally, the wavelength-dependent propagation loss was obtained from cutback measurements, revealing the role of Si absorption and polarizations in the sidewall scattering loss. Our study shows the effect of loss reduction due to Si over-etch in Ge-on-Si photonics waveguide devices, thus allowing for reduction of Ge-on-Si bending radius and enabling miniaturization of the sensing footprint. The results obtained will provide insights towards miniaturizing Ge-on-Si waveguide sensing devices. Future work would include controlling incident polarization for more precise waveguide loss and sensing characterizations.

ACKNOWLEDGEMENTS

This research is supported by Agency for Science, Technology and Research (C220415015) for design and fabrication and the National Research Foundation, Singapore, and A*STAR (Agency for Science, Technology and Research), Singapore under its Low-Carbon Energy Research (LCER) Funding Initiative (FI) (Award no.: U2102d2012) for testing and analysis.

REFERENCES

[1] Popa, D. and Udrea, F., "Towards Integrated Mid-Infrared Gas Sensors," Sensors 19(9), 2076 (2019).

[2] Tan, X., Zhang, H., Li, J., Wan, H., Guo, Q., Zhu, H., Liu, H. and Yi, F., "Non-dispersive infrared multi-gas sensing via nanoantenna integrated narrowband detectors," Nat Commun 11(1), 5245 (2020).

[3] Ng, D. K. T., Xu, L., Fu, Y. H., Chen, W., Ho, C. P., Goh, J. S., Chung, W. W., Jaafar, N., Zhang, Q. and Lee, L. Y. T., "CMOS AlN and ScAlN Pyroelectric Detectors with Optical Enhancement for Detection of CO_2 and CH_4 Gases," Adv. Electron. Mat. 9, 2300256 (2023).

[4] Ng, D. K. T., Ho, C. P., Xu, L., Chen, W., Fu, Y. H., Zhang, T., Siow, L. Y., Jaafar, N., Ng, E. J., Gao, Y., Cai, H., Zhang, Q. and Lee, L. Y. T., "NDIR CO_2 gas sensing using CMOS compatible MEMS ScAlN-based pyroelectric detector," Sensors and Actuators: B. Chemical, 346, 130437 (2021).

[5] Ng, D. K. T., Xu, L., Chen, W., Wang, H., Gu, Z., Chia X. X., Fu, Y. H., Jaafar, N., Ho, C. P., Zhang, T., Zhang, Q. and Lee, L. Y. T., "Miniaturized CO_2 Gas Sensor Using 20% ScAlN-based Pyroelectric Detector," ACS Sensors, 7, 2345-2357 (2022).

[6] Mashanovich, G. Z., Mitchell, C. J., Penades, J. S., Khokhar, A. Z., Littlejohns, C. G., Cao, W., Qu, Z., Stankovic, S., Gardes, F. Y., Masaud, T. Ben, Chong, H. M. H., Mittal, V., Murugan, G. S., Wilkinson, J. S., Peacock, A. C. and Nedeljkovic, M., "Germanium Mid-Infrared Photonic Devices," Journal of Lightwave Technology 35(4), 624–630 (2017).

[7] Nedeljkovic, M., Penades, J. S., Mittal, V., Murugan, G. S., Khokhar, A. Z., Littlejohns, C., Carpenter, L. G., Gawith, C. B. E., Wilkinson, J. S. and Mashanovich, G. Z., "Germanium-on-silicon waveguides operating at mid-infrared wavelengths up to 8.5 µm," Opt Express 25(22), 27431 (2017).

[8] Gallacher, K., Millar, R. W., Griškevičiūte, U., Baldassarre, L., Sorel, M., Ortolani, M. and Paul, D. J., "Low loss Ge-on-Si waveguides operating in the 8–14 µm atmospheric transmission window," Opt Express 26(20), 25667 (2018).

[9] Kozak, D. A., Stievater, T. H., Mahon, R. and Rabinovich, W. S., "Germanium-on-Silicon Waveguides at Wavelengths From 6.85 to 11.25 microns," IEEE Journal of Selected Topics in Quantum Electronics 24(6), 1–4 (2018).

[10] Chang, Y.-C., Paeder, V., Hvozdara, L., Hartmann, J.-M. and Herzig, H. P., "Low-loss germanium strip waveguides on silicon for the mid-infrared," Opt Lett 37(14), 2883 (2012).

[11] Lim, L. W., Fong, A. W. K., Ang, R. C. F., Voo, R. Q. G., Teh, J. N. H., Md Husni, Md H. K., Cai, H., Tobing, L. Y. M., Li, N., Chung, S. and Lee, L. Y. T., "Reduction of Ge-on-Si waveguide propagation loss by laser and hydrogen annealing," Proc. SPIE 12424, Integrated Optics: Devices, Materials, and Technologies XXVII, 1242414 (2023).